LA-UR- *09-00055*

Title: | Forced Convection and Transport Effects during Hyperbaric Laser Chemical Vapor Deposition

Author(s): | James L. Maxwell, Marcie Black, Craig Chavez, Karlene Maskaly, Miguel Espinoza

Intended for: | Applied Physics A

Los Alamos
NATIONAL LABORATORY
——— EST.1943 ———

Forced Convection and Transport Effects during Hyperbaric Laser Chemical Vapor Deposition

James L. Maxwell,* Marcie Black, Craig Chavez, Karlene Maskaly, Miguel Espinoza
NEMISIS Team, IAT-2, Los Alamos National Laboratory, Los Alamos, NM, USA,

Mats Boman
Inorganic Chemistry, Angstrom Laboratory, Uppsala University, Uppsala, Sweden.

*Corresponding Author: MS: J566, DP: 01S, Los Alamos, NM 87545, USA,
E-mail: jmaxwell@lanl.gov, Fax: 505-665-6389.

Abstract

This work explores mass transport processes during HP-LCVD, including the transverse *forced-flow* of precursor gases through a nozzle to enhance fiber growth rates. The use of laser trapping and suspension of nano-scale particles in the precursor flow is also described, providing insights into the nature of the gas flow, including jetting from the fiber tip and thermodiffusion processes near the reaction zone. The effects of differing molecular-weight buffer gases is also explored in conjunction with the Soret effect, and it is found that nucleation at the deposit surface (and homogeneous nucleation in the gas phase) can be enhanced/ retarded, depending on the buffer gas molecular weight. To demonstrate that extensive microstructures can be grown simultaneously, three-dimensional fiber arrays are also grown *in-parallel* using diffractive optics--without delatory effects from neighboring reaction sites.

Keywords:
Laser Deposition, Hyperbaric Pressure, Natural Convection, Forced Flow

1 Introduction

Hyperbaric laser chemical vapor deposition (HP-LCVD) uses a focused laser beam to deposit three-dimensional microstructures from gas-phase precursors (at pressures above one atmosphere) [1]. If the laser beam is held stationary, a deposit may grow away from the substrate and along the beam axis forming a fiber or rod [2-3]. The orientation of the beam can also be changed during growth to form complex three-dimensional structures in a freeform manner [4-7]. The carbon fiber array and tapered coils of Fig. 1 were all grown using this approach; each was deposited in a matter of minutes, excluding manual alignment/set-up times. In Fig. 1A, fibers were grown in the direction of a stationary laser beam, while the coils of Fig. 1(B)-(D) were grown by continuously rotating and translating the fibers relative to the beam, while at the same time modulating the radius of rotation. The more rapidly such microstructures can be fabricated, the more practical the HP-LCVD process becomes for industrial use.

Growth rates of fibers and microstructures during HP-LCVD are often *mass-transport limited (MTL)* [1]; i.e. they are grown at the maximum rate at which reactant molecules can arrive at the reaction zone. The magnitude of this mass transport limit changes dramatically with precursor pressure. At low pressures, where the mean free path is large, gas molecules transport diffusively to/from the reaction zone. As the pressure rises, however, a boundary

layer forms around the reaction zone, and a natural convective plume develops within the surrounding bulk fluid. The bouyancy of this convective plume is driven by heat released from the reaction zone, both through energy absorbed from the incident beam and from heat emitted by the reaction itself (exothermic reactions). In previous work, we have observed very rapid convection past the reaction zone (>14 cm/s) [8-9], using nanoparticles to track the fluid flow rates. The greater the pressure in the chamber, the greater the velocity of this convective plume, and the thinner the boundary layer becomes. Ultimately, this raises the MTL and allows more rapid growth. Hence, the process is most practical at hyperbaric pressures (i.e. >1 bar).

HP-LCVD work to date has largely been conducted either: (1) with some nominal *undirected* flow through a chamber to prevent build-up of by-products, or (2) under "static-pressure" conditions in a chamber sufficiently large that by-products can only build to negligible concentrations. In these cases, natural convection has been the dominant mode of mass transport. In very small chambers, however, the natural convective plume described above
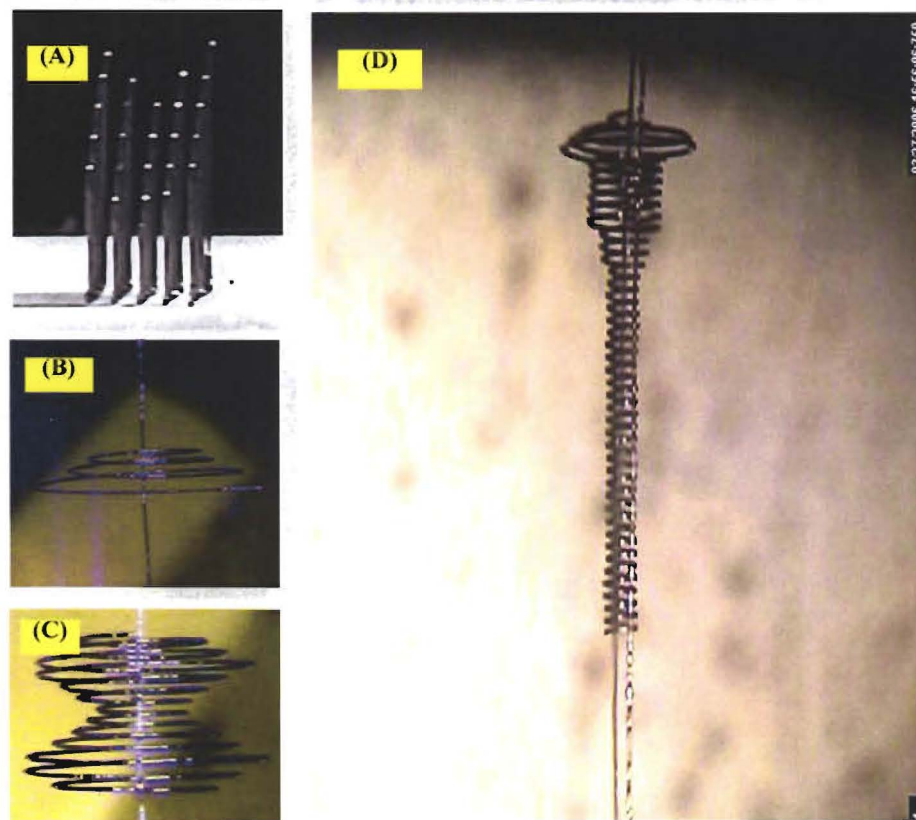

Fig. 1: (A) A Fiber Array of carbon probes grown using HP-LCVD. Each fiber is approximately 40 μm in diameter. Such arrays can be used for many purposes, including field emitters, sensors, and micro-scale probes. (B)-(D) Tapered microcoils, hourglass springs, and complex structures grown by HP-LCVD. Such devices can be useful as sub-millimeter mechanical springs or electrical coils. Note that the coil pitch and radius can be controlled independently, while the fiber diameter is largely determined by the laser power and precusor pressures employed. By combining these two basic elements, more complex three-dimensional structures and micro electro mechanical systems (MEMS) can be created.

can wrap around itself, creating a convective cell that builds to a steady velocity. We have previously seen that this mixed natural-forced convection can indeed enhance fiber growth rates [10]. True forced convection, localized near the growth zone through the use of a micro nozzle (i.e. blowing gas across the reaction zone), was first proposed in 1996 as a tool to enhance growth rates during HP-LCVD [11]. It has been attempted by several authors [12-14] with varied results, and there has been some question regarding its utility.

Several additional transport phenomena have been observed during HP-LCVD that have yet to be fully-documented and explained; in previous articles, we have observed the formation of microvortices emanating from the reaction zone [9], measured the shape and thickness and the boundary layer surrounding fibers [15, 9], and observed counter-rotating flows during growth [9]. However, one phenomena that has not yet been fully explored is the development of a strong outflow from the reaction zone, not in the direction of natural convection, but along the laser axis (and into the beam). Some evidence for this phenomenon has been seen during nearly all HP-LCVD experiments [16], but it is often difficult to document, due to the rapid flow of the precursor during high-speed growth. Another phenomena is the appearance of "stationary" particles in the flow, that remain for long time periods in front of an evolving fiber, but are rapidly swept away as conditions change or they are disturbed from their position. Finally, we have observed that the addition of buffer gases can have a strong effect on the shape and microstructure of the resulting fibers, and can aid in achieving 3-D growth with precursors that have low vapor pressures or with deposit materials that melt at low temperatures.

Consequently, the primary objectives of this work were: (1) to demonstrate conclusively that forced convective flow through a micro nozzle can indeed lift the MTL and enhance fiber growth rates; (2) to explore mass transport phenomena during HP-LCVD, e.g. jetting, that can affect the boundary layer and the MTL; and (3) to investigate the effects of buffer gases on mass transport and deposit microstructure.

2 Experimental

For the forced flow experiments, a 1.6 mm ID stainless-steel nozzle was held horizontally, transverse to the growth direction of the (horizontally-grown) fibers, and perpendicular to the natural convective plume, as illustrated in Fig. 2(A). The nozzle outlet was at a distance of 2 mm from the fiber tip. A gas pressure regulator was employed at the inlet to this nozzle, to maintain a constant upstream pressure. The downstream pressure inside the chamber was also maintained constant using a manual needle valve, so the ratio of natural convection to forced convection could be controlled.. The beam waist was placed directly across from the nozzle, with the substrate 300 microns behind this point, so each fiber was grown within the steady-state regime and at the optimal focus as it passed by the nozzle, giving a "peak" growth rate. An Ar+ laser was used at the primary lines of 488/514 nm. Additional details of the HP-LCVD apparatus can be found in previous articles [1, 10].

3 Results and discussion

Forced Convection

In Fig 2(B), we provide evidence of forced convection growth rate enhancements, using the horizontal nozzle described previously. By controlling the precursor mass flow rate and
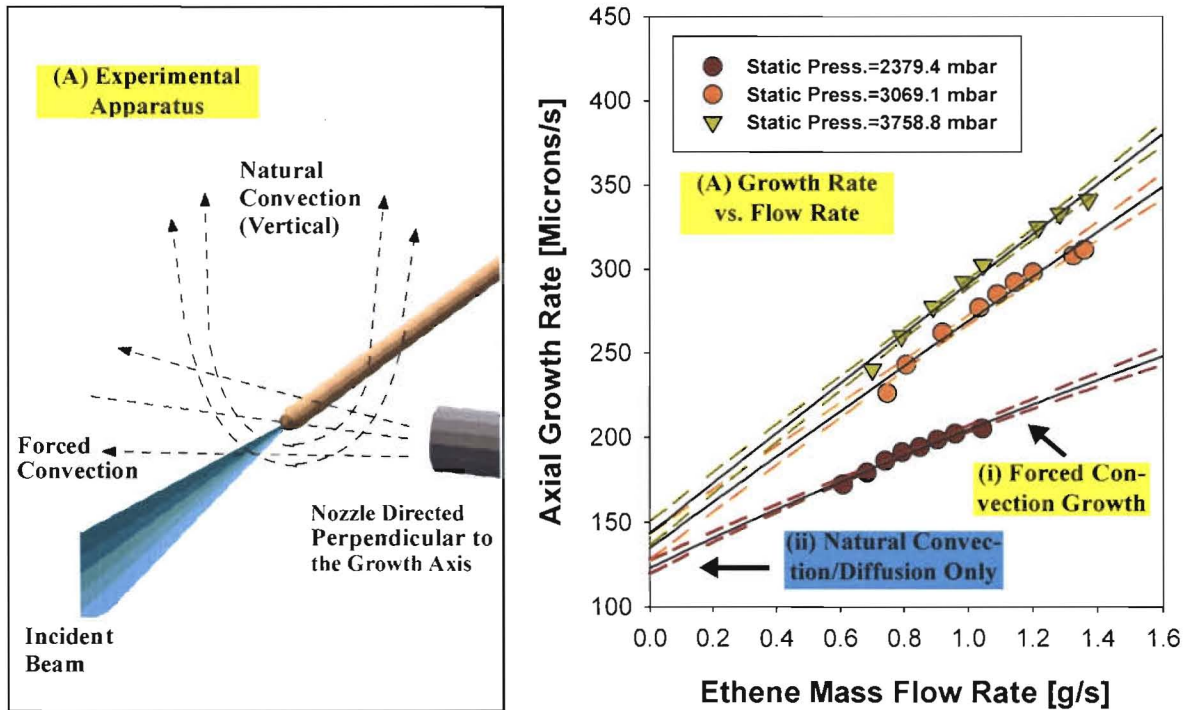
Fig. 2: Forced convection can be used to enhance the axial growth rates of fibers. This figure illustrates the relative contributions of natural convection and forced convection on the axial fiber growth rate. The experimental apparatus is shown in Fig. 6A, where a nozzle supplies fresh precursor directly to a growing fiber during steady-state growth. The nozzle is oriented horizontally and transverse to the fiber growth direction (and normal to the direction of natural convection). Three different static (chamber) pressures are shown in Fig. 6B, where the mass flow rate varies through the nozzle. Both modes of convection contribute to the growth rate; however, in this case, the forced convective flow (i) enhances the growth rate by 1.5-3.0x. Note that the individual graphs converge to the expected steady-state growth rate with no flow, i.e. where natural convection dominates (ii). In this case, ethene was the precursor, carbon was the deposit material, and the incident cw laser power was held constant at about 285 mW.

the chamber pressure simultaneously, we are able to distinguish the contributions of natural convection HP-LCVD vs. forced flow, nozzle-based HP-LCVD. Three different static chamber pressures of ethylene are shown with varying mass flow rates through the nozzle. The cw laser power was held constant at 285 mW for all of the data points, and the measured values are the peak growth rates. Each increase in base pressure brings with it an increase in axial growth rate (as expected from previous results using only natural convection) [3, 1, 17]. However, note that the *forced* flow of precursor through a nozzle increases the axial growth rates by a factor of 1.5-3.0X at the highest flow rates, and that the curves extrapolate very closely to values previously reported for natural convection at the no-flow condition (i.e. y-axis intercept) [1]. Clearly, further growth rate enhancements are possible by increasing the mass flow rates, in addition to the base pressures.

Interestingly, while the transport rate is clearly enhanced with forced flow, one would expect the directed flow to also cool the fiber—and hence (eventually) lower the deposition rate; this effect was hardly observed at the flow rates employed, presumably because the fiber

Base Pressure, P_o [mbar]	Axial Rate with no Flow, r_o[μm/s]	Exponential, ζ
2379.4	122.76±1.58	0.735±0.022
3069.1	134.62±3.15	0.996±0.03
3758.8	143.28±2.83	1.020±0.03

Table 1: Forced Convective Flow: Rate Constants and Exponentials

tips were sufficiently within the mass-transport limited regime that kinetics could not yet apply. However, at some critical mass flow rate(s), still to be determined, the axial growth rate should level off (and eventually drop) once a fiber tip enters the kinetically-limited regime. Of course, this could be counter-acted by increasing the laser power, so higher flow rates may continue to be employed. The slight convex shape of the three data curves in Fig. 6, may be related to this effect. To determine the degree of curvature, each set of data was fit to the equation:

$$r = r_o \left(1 + \dot{m}\right)^{\zeta}$$

where r is the growth rate, r_o is the growth rate with only natural convection, $\dot{m}$ is the mass flow rate of precursor, and ζ is the exponential to be determined. The results for each data set are given in Table 1, with 95% confidence level curves provided in Fig. 6B (dotted lines). The non-linear regression coefficients of determination (r^2) for each data set are all ≥97%. Observe that the curves are increasingly linear (i.e. $\zeta \rightarrow 1$) as the static chamber pressure rises, and the reaction becomes more deeply mass transport limited. Further experiments, at greater flow rates will be necessary to determine the point(s) at which the fibers will cool enough to enter the kinetic regime. However, this experimental approach provides a simple route to determine the MTL-->kinetic transition that can be used in the future.

Transport Effects during HP-LCVD

An important observation during fiber growth relates to the motion of gases near the reaction zone. We have long suspected that a rapid outflow along the laser axis may emanate from the reaction zone during HP-LCVD, but at customary growth rates, it has proven difficult to measure the fluid direction/velocity near the fiber tip using particle image velocimetry (PIV).

To investigate this further, a series of boron-doped silicon fibers were grown, using a mixture of trimethylboron and disilane, where B-Si particles could be readily generated in the gas-phase. After growing a short fiber at high powers (>1W), and generating particles in the gas flow, the laser power was lowered to 120mW, and offset transverse to the fiber axis by about 10 microns. Using single-beam (gradient) laser trapping [18-22], several micron-scale particles were soon captured near the laser focus, and their motion was recorded using video microscopes.

Two interesting video sequences are shown in Fig. 3. Note that in all frames, the laser beam is directed toward the right, and inpinges on a newly initiated fiber at right angles to a tungsten wire (substrate). The laser focus (w_o) is indicated at the fiber tip. Nanoparticles can be seen in the converging laser beam, and some have collected on the tungsten wire. Two

Fig. 3: Motion of Nanoparticles in the Fluid Flow
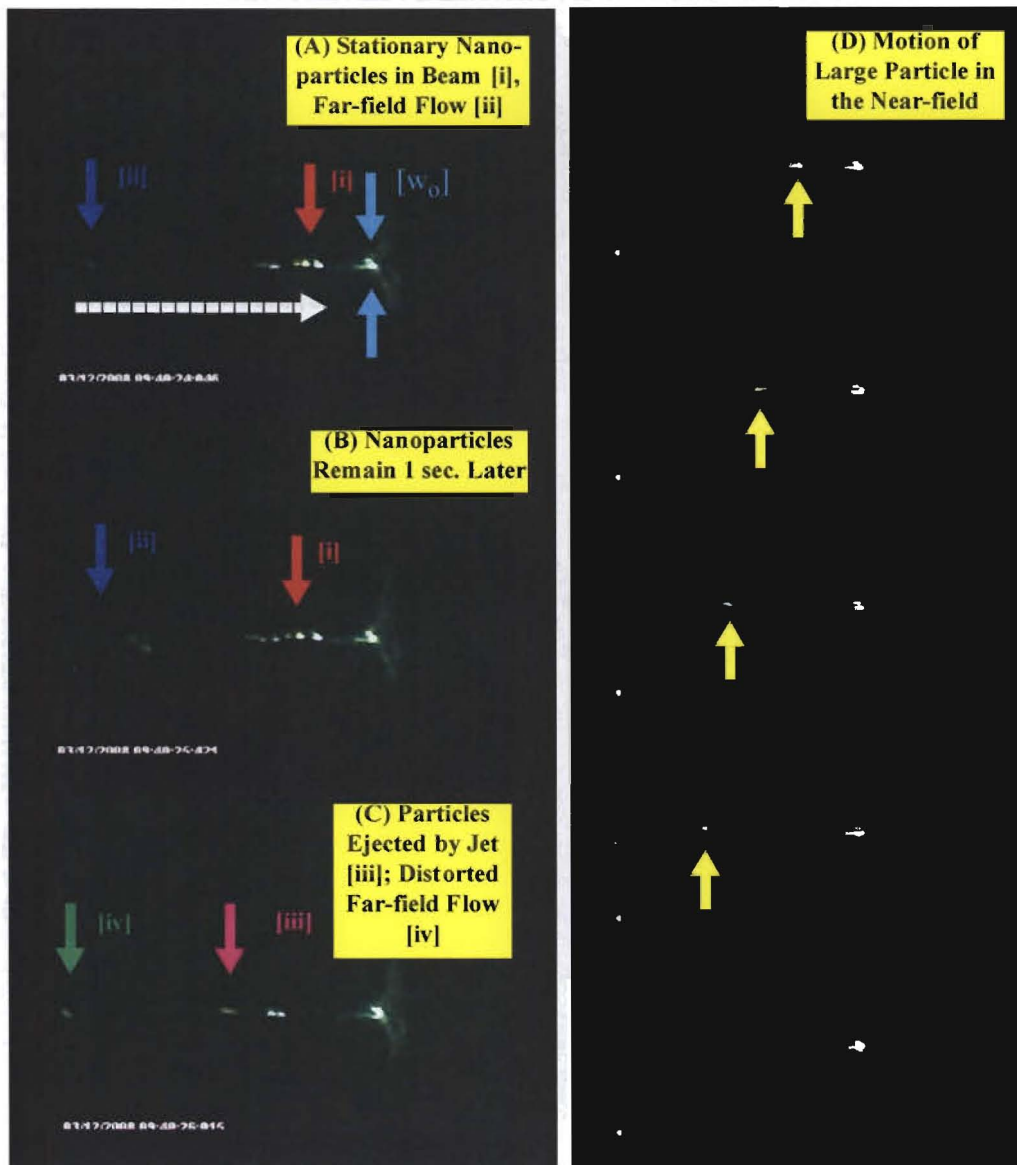
regimes are apparent in all the video frames, one near the fiber tip (i), the "near-field," and one on the left-hand edge of the frame (ii), the "far-field." The far-field is where the free-stream convective flow is active, as close-up views show the nanoparticles in rapid motion diagonally to the lower-right. There is also some evidence of particles moving axially along the laser axis in the far-field.

The first video sequence, Fig. 3(A)-(C), gives three frames, the uppermost frame being the first. Observe the 6-7 stationary particles in the near-field of frames (A) and (B). These appear to hover in the fluid, occasionally moving slightly to the left or right, but apparently isolated from the free-stream flow. Just prior to frame (C), the laser beam is adjusted slowly

toward the fiber tip, and as fiber growth recommenses, the trapped particles are almost immediately ejected away from the fiber toward the far-field (iii). While scattered light from the fiber tip (back up the laser axis) may partially interrupt the laser trap, it is most likely that a strong fluid outflow develops from the reaction at the fiber tip, and the force on the particles becomes unbalanced. This outward "jet" also apparently distorts the far-field flow (iv), moving it outward and changing the motion of some particles in the flow.

A second sequence of frames, Fig. 3(D), shows the entry of a large particle into the near-field with the laser beam aligned with the fiber tip, but at lower powers, <100mW. In this case, the particle is not precisely balanced by the laser trap and is ejected away from the fiber tip, presumably by an out-flow of fluid (toward the left). However, in the third and fourth frames, the particle appears to be decelerating as it approaches the far-field, while in the last frame, it has appearently been swept away by the far-field flow.

The exact cause of this outflow is unknown at this time, but is likely the generation of high-temperature byproducts in the reaction zone, where a very large temperature gradient exists. The very tip of the fiber, where the surface is normal to the laser axis, is at the highest temperature by far, so the explanding gas is driven normal to the surface (and into the beam).

Clearly, any model of HP-LCVD will need to address these elements of mass transport to fully describe the process, as the convective-flow boundary layer may be distorted by this outflow. Interestingly, there are often volcano-like structures at the tip of fibers. Many expanations have been provided for this structure over the years, including transport limitations, thermodynamic limitations, temperature-dependent sticking coefficients, melting, or ablation at the fiber tip [23-27]. It is possible, however, that the outflow seen in Fig. 3 could contribute to the formation of volcano-like structures by preventing the entrance of fresh precursor at the very center of the reaction zone.

Thermal Conductivity and Molecular Weight of the Gas Mixture

At hyperbaric pressures, gas convection not only establishes a necessary heat balance for steady-state growth [28], but it also enhances the transport of the precursor to the reaction zone, thereby increasing the axial growth rate. An added benefit of greater precursor pressures is that the grain size of the deposit generally becomes more fine, as adatoms have less time to rearrange to optimal crystal sites [24, 29-30]. Consider, for example, the tungsten fibers of Fig. 4(A)-(B), grown from low-pressure and hyperbaric mixtures of WF_6 and H_2; at WF_6 partial pressures of 350 mbar, single crystal fibers were obtained (A). At hyperbaric pressures, however, the microstructure became polycrystalline, eventually yielding grain sizes of only 2-3 microns at 1500 mbar WF_6 partial pressures and above (B).

It is not just the partial pressure of the precursor system that matters, however. An important discovery was that the fiber diameter and deposit morphology could be controlled independently through the addition of particular buffer gases, allowing for instance, an optimal growth temperature and fiber diameter to be maintained at a particular laser power, while changing the deposit internal structure at will. This is especially useful for precursor gases that are available only within a limited pressure range--or that have very low vapor pressures. For example, if WF_6 were to decompose before reaching a pressure of 1500 mbar, it would not have been possible to grow the polycrystalline fiber of Fig. 4(B). There are many precursor systems that are limited in this fashion.

Thus, to explore the effects of inert gases on deposit microstructure, several experiments were carried out, using W-fiber growth as the model. The first was the addition of helium to a WF_6/H_2 mixture, in 50 mbar steps. Due to helium's high thermal diffusivity/conductivity, a marked cooling effect was observed, where heat was drawn from the reaction zone into the gas-phase. This simultaneously increased gas-phase nucleation while broadening the initial fiber diameter--through additional nucleation sites on both substrate and fiber. As the He-pressure increased, the microstructure became more polycrystalline, and when over 200 mbar of helium was introduced, homogeneous nucleation was observed at distances of several hundred microns from the growth zone. At helium partial pressures of 500 mbar or more, it was not possible to initiate fiber growth, unless the laser power was greatly increased. Importantly, this heat transfer is also enhanced through the Soret effect [31-32, 10], where light molecular weight gases (e.g. He) are concentrated near the heated fiber tip, greatly enhancing the thermal conductivity of the gas mixture near the reaction zone.

To observe the opposite effect, several noble gases were also attempted with increasing molecular weights (Ar, Kr, and Xe), and their partial pressures were increased in 50 mbar increments. In contrast to He, the use of these gases produced deposits that were much more well-defined, and the observed gas-phase nucleation decreased with increasing buffer gas molecular weight. This is to be expected, as the gas thermal diffusivities/conductivities drop with increasing mass; xenon, for example, has a thermal diffusivity 1/6th that of helium, and gas-phase nucleation was almost absent with this gas. This approach can be extrapolated to even higher-molecular weight inert gases, of similar or even greater mass than the precursor itself, e.g. SF_6, which can be used to effectively lower the thermal conductivity of the gas mixture and insulate the growth zone.

The use of high molecular weight inert gases will allow the growth of finer fiber diameters and suppress unwanted homogeneous nucleation in future growth experiments. It will also permit the resulting microstructure to be decoupled from the fiber diameter, which heretofore has been controlled by the laser power and precursor pressure. Finally, many low-vapor pressure precursors can now be explored for fiber growth, using hyperbaric inert gases to sustain adequate convection. **I**

Mass Transport Effects during Parallel Growth

Ultimately, for HP-LCVD to be a practical tool for microfabrication, it is important to be able to grow many fibers at once. We have recently grown bundles of 3, 5, 25, and 49 fibers simultaneously using diffractive optical elements to generate multiple laser foci. These were grown horizontally, while rotating the diffractive optic to intertwine the fibers as they are grown. An example of this can be seen in Fig. 5, where a bundle of 49 Al-fibers is shown during growth.

An important question is the extent to which each reaction zone affects adjacent sites. At high laser powers, some homogeneous nucleation normally occurs near each reaction zone, and byproducts are generated at each site. With fiber spacings as small as 300 microns apart, we have yet to see significant changes in fiber compositions or growth rates from that of single fibers. Of course, as we have learned, high molecular weight buffer gases could be used to inhibit diffusion and homogeneous nucleation far from the reaction zone(s) were this a problem.

Fig. 4: The effects of precursor and buffer gas partial pressures on the microstructure of tungsten fibers grown under various conditions: (A) At WF_6 partial pressures of 350 mbar, single crystals of tungsten could be grown. (B) At much higher WF_6 pressures (1500 mbar), fine-grained polycrystalline fibers were obtained. In (C)-(E), identical conditions were used for each fiber, except that increasing amounts of helium were added as a buffer gas. This resulted in increased heat transfer to the surrounding gas mixture and increased homogeneous nucleation in the gas-phase--eventually broadening the initial fiber diameter (E). In a similar way, it was demonstrated that the gas mixture thermal conductivity (and resulting gas-phase nucleation) can be suppressed through the addition of higher molecular weight inert gases, such as krypton and xenon. This technique can be extrapolated to even higher molecular weight gases, e.g. SF_6, that play no role in the reaction, but help control the resulting microstructure. The approach can also be used to support the growth of fibers from low-vapor pressure precursors, where the fiber would ordinarily melt during growth.
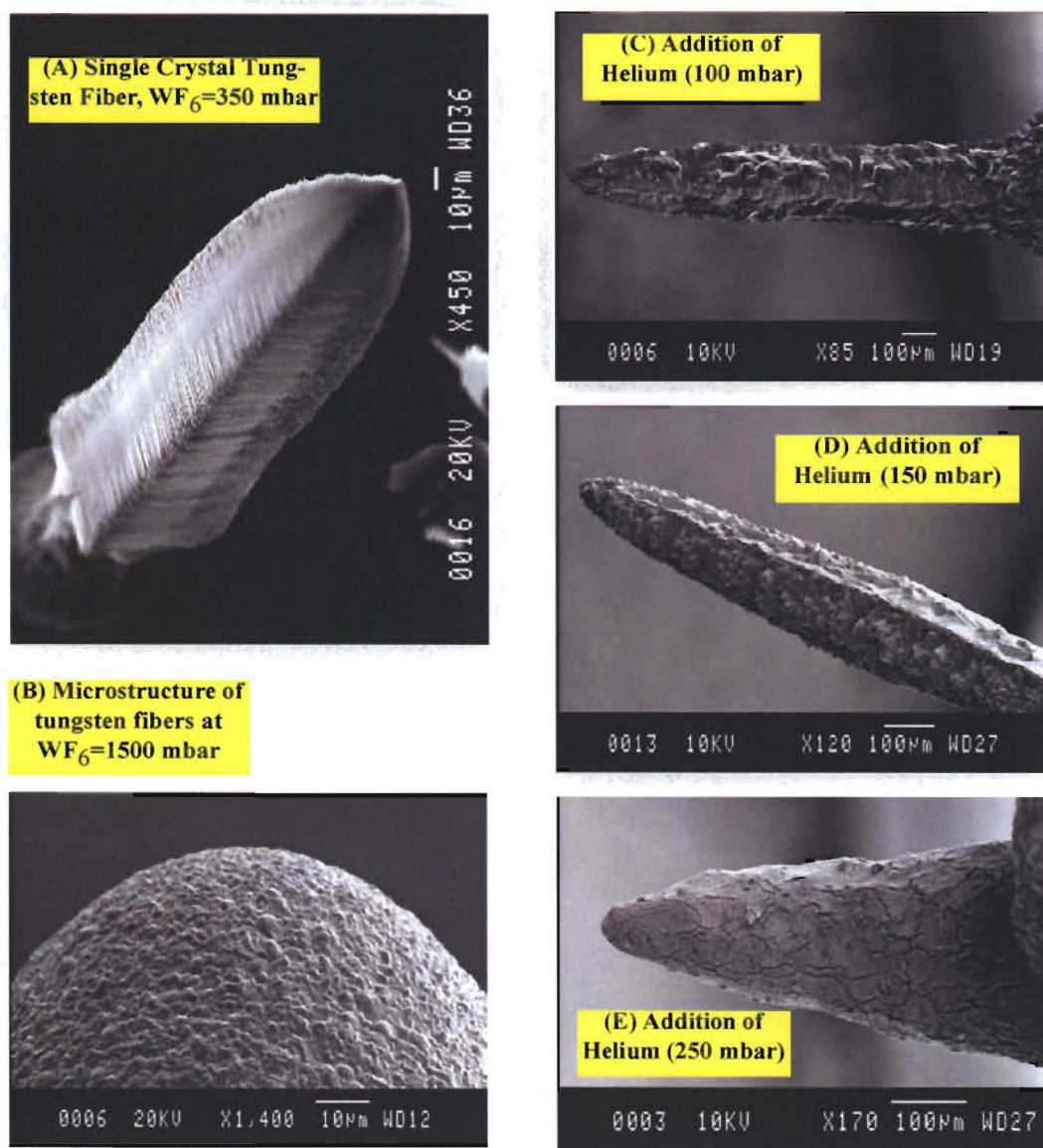
Conclusions

We have demonstrated that forced convection can indeed be used to enhance fiber growth rates, provided the nozzle is oriented in a direction that does not inhibit natural convection at the fiber tip. We have also observed important outflows or "jetting" from the fibers during growth that certainly affect the transport of reactants to the fiber and the shape of the convective boundary layer surrounding the reaction zone. We have found that the addition of high-molecular weight buffer gases of low thermal conductivity can reduce homogeneous nucleation and decouple the fiber diameter from the incident laser power and fiber crystal structure, so that fiber properties can be better tailored to their end application. Finally, we were able to demonstrate that parallel fiber growth is possible without contaminating adjacent reaction sites down to 300 micron fiber spacings.

Fig. 5: Parallel Growth Example.

(A) 7x7 Arry of Parallel Fibers Growing Simultaneously
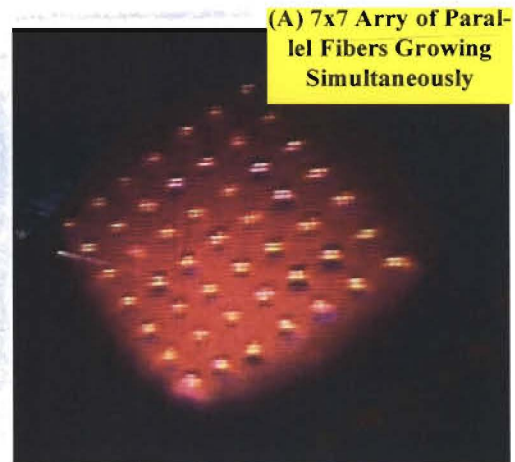
4   References

1. J. L. Maxwell, M. Boman, R. W. Springer, A. Nobile, K. DeFriend, L. Espada, M. Sandstrom, D. Kommireddy, J. Pegna, D. Goodin, Adv. Func. Mater., **15** (7), 1077-1087 (2005).

2. H. Westberg, M. Boman, J. O. Carlsson, J. de Physique IV, **3** (C3), 225-232 (1993).

3. F. T. Wallenberger, P. C. Nordine, Science, **260** (5104), 66-68 (1993).

4. M. Boman, D. Bauerle, J. Chin.,, Chem. Soc. **42,** 405 (1995).

5. M. Boman, H. Westberg, S. Johansson, J. Schweitz, IEEE Micro Electro Mechanical Systems Workshop, Travemuende, Germany, 162-167 (1992).

6. J. Maxwell, *Three-Dimensional Laser-Induced Pyrolysis: Modelling, Growth Rate Control, and Application to Mcro-Scale Prototyping,* Ph.D. Thesis, Rensselaer Polytechnic Institute, Troy, NY, 232 (1996).

7. O. Lehmann, M. Stuke, Mater. Lett., **21** (2), 131-136 (1994).

8. J. Maxwell, *Three-Dimensional Laser-Induced Pyrolysis: Modelling, Growth Rate Control, and Application to Micro-Scale Prototyping,* Ph.D. Thesis, Rensselaer Polytechnic Institute, Troy, NY, 190-191 (1996).

9. J. L. Maxwell, C. A. Chavez, R. W. Springer, K. R. Maskaly, D. Goodin, Diam. & Rel. Mater., **16,** 1557-1564 (2007).

10. J. L. Maxwell, M. Boman, R. W. Springer, J. Narayan, S. Gnanavelu, J. Am. Chem. Soc., **148** (13), 4411.

11. J. L. Maxwell, J. Pegna, U.S. Patent #5,786,023.

12. J. Pegna, Freeform Fibers, Inc.

13. W. J. Lackey, D. Jean, C. Duty, R. Johnson, S. Bondi, Carbon, **40**, 1435 (2002).

14. C. Duty, R. Johnson, J. Gillespie, A. Fedorov, W. J. Lackey, Appl. Phys. A, 77, 697-705 (2003).

15. J. Maxwell, *Three-Dimensional Laser-Induced Pyrolysis: Modelling, Growth Rate Control, and Application to Micro-Scale Prototyping,* Ph.D. Thesis, Rensselaer Polytechnic Institute, Troy, NY, 174 (1996).

16. J. Maxwell, *Three-Dimensional Laser-Induced Pyrolysis: Modelling, Growth Rate Control, and Application to Micro-Scale Prototyping,* Ph.D. Thesis, Rensselaer Polytechnic Institute, Troy, NY, 190 (Fig. 6-27, frame B), (1996).

17. J. L. Maxwell, M. R. Black, C. A. Chavez, K. R. Maskaly, M. Espinoza, M. Boman, L. Landstrom, Appl. Phys. A, **91**, 507-514 (2008).

18. Z. Ding, G. Lai, T. Sakakibara, S. Shinohara, J. Appl. Phys., **88** (2), 737-741, (2000).

19. A. Jonas, L. Sramek, M. Liska, P. Zemanek, SPIE Proc. NACMO '97, **3580**, 91-101 (1998).

20. Y. K. Nahmias, D. J. Odde, IEEE J. Quantum Electronics, **38** (2) 131-141 (2002).

21. T. A. Nieminen, H. Rubinsztein-Dunlop, N. R. Heckenberg, J. Quantitative Spectroscopy and Radiative Transfer, **70**, 627-637 (2001).

22. S. Chu, Science, **253** (5022), 861-866 (1991).

23. S. D. Allen, A. B. Tringubo, J. Appl. Phys. **54**, 1641-1643 (1983)

24. J. Bloch, Y. Zeiri, R R. Lucchese, Surf. Sci., **257**, 402-416 (1991).

25. J. Mazumder, A. Kar, Theory and Application of Laser Chemical Vapor Deposition, Plenum, 275-283 (1995)

26. D. Bauerle, *Laser Processing and Chemistry, 2nd Edition,* Springer-Verlag, 317-318 (1996).

27. H. Westberg, M. Boman, A.-S. Norekrans, J. -O. Carlsson, Thin Solid Films, **215**, 126-133 (1992).

28. J. Maxwell, *Three-Dimensional Laser-Induced Pyrolysis: Modelling, Growth Rate Control, and Application to Micro-Scale Prototyping,* Ph.D. Thesis, Rensselaer Polytechnic Institute, Troy, NY, 114-116, (1996).

29. J. Elders, J. D. W. Van Voorst, Appl. Surf. Sci., **54**, 135-140 (1992).

30. H. Westberg, M. Boman, J.-O. Carlsson, Thin Solid Films, **218**, 8-14 (1992).

31. S. Duhr, D. Braun, Proc. Natl. Acad. Sci. USA, **104**, 3-4 (2007).

32. D. Bauerle, *Laser Processing and Chemistry, 2nd Edition,* Springer-Verlag, 312-313 (1996).